Appl Petrochem Res (2015) 5:71–80
DOI 10.1007/s13203-014-0090-x

ORIGINAL ARTICLE

# Catalytic functionalities of Pd catalysts supported on spinel $MgAl_2O_4$ for coupling of ethylbenzene dehydrogenation with nitrobenzene hydrogenation

**Yengaldas Harikrishna · Vanama Pavan Kumar · Kuna Ramu · Komandur V. R. Chary · Vattikonda Venkat Rao**

Received: 14 August 2014 / Accepted: 29 September 2014 / Published online: 17 October 2014


**Abstract** Direct coupling of oxidative dehydrogenation of ethylbenzene with nitrobenzene hydrogenation in a fixed-bed catalytic reactor at atmospheric pressure in the temperature range of 673–823 K over $MgAl_2O_4$-supported palladium catalysts has been investigated. Simple dehydrogenation of ethylbenzene (DHEB) is reversible, endothermic and thermodynamically limited. The continuous removal of co-produced hydrogen in DHEB for in situ hydrogenation of nitrobenzene over $Pd/MgAl_2O_4$ catalyst improves the performance of the DHEB process. A series of Pd (0.25–4.0 wt%) catalysts supported on $MgAl_2O_4$ was prepared. The catalyst samples were characterized by X-ray diffraction (XRD), $H_2$-Temperature-programmed reduction (TPR), X-ray photoelectron spectroscopy (XPS), Transmission electron microscopy (TEM), CO chemisorption, $CO_2$–Temperature-programmed desorption and BET surface area. Dispersion and particle size of Pd were obtained by CO chemisorption. The reaction profile shows that palladium (0.5 wt%) is an optimum loading to get maximum conversion of ethylbenzene (51.8 %) and nitrobenzene (47.3 %) to give 91.4 and 100 % selectivity of styrene and aniline, respectively.

**Keywords** $MgAl_2O_4$ spinel · Dehydrogenation · Hydrogenation · Ethylbenzene and nitrobenzene

Y. Harikrishna · V. Pavan Kumar · K. Ramu · K. V. R. Chary · V. Venkat Rao (✉)
Catalysis Division, CSIR-Indian Institute of Chemical Technology, Hyderabad, India
e-mail: vattikondav@yahoo.com

## Introduction

A large number of important processes in the chemical and petrochemical industries have reactions which are, to a greater or lesser extent, limited by equilibrium considerations. Production of styrene is one of such processes. It is a major petrochemical commodity used for the production of many different polymeric materials, such as acrylonitrile–butadiene–styrene (ABS), styrene–acrylonitrile (SAN), styrene–butadiene rubber (SBR), etc. [1]. Its number of applications and demand are still growing. It is commercially produced by vapor-phase dehydrogenation of ethylbenzene (DHEB) with large excess of superheated steam over potassium promoted iron oxide (Fe–K–O) catalyst in the temperature range of 873–973 K [2]. The main drawback of this process is its strongly endothermic character and limited equilibrium conversion of ethylbenzene [3]. Several approaches were being attempted by reducing the amount of co-produced hydrogen in the product to improve the performance of styrene yield either through reactor design or process modifications [4, 5]. The former approach involving mostly membrane reactors has limited applicability due to their sensitivity towards certain species present in the reaction and also a cost factor. The other approach involves the introduction of oxidant molecules such as oxygen, halogens, sulfur and more recently mild oxidant like $CO_2$ in the dehydrogenation of ethylbenzene to overcome thermodynamic constraints [6–8]. However, development of commercial process was not successful to manufacture styrene by oxidative DHEB because of loss of styrene selectivity in addition to safety factors. Towler and Lynn reported that direct coupling of endothermic and exothermic reactions had improved thermal efficiency, reduction in catalyst deactivation and reaction rate due to displacement of equilibrium [9]. Similarly, Bautista as well

as Sun et al. [10, 11], also reported the improved performance of conversion of ethylbenzene into styrene in the presence of nitrobenzene overcoming thermodynamic equilibrium constraints in consistent with the Le Chatelier–Braun principle. However, separation of products and recycling of reactants in direct coupling reaction may require additional unit operations. In practice, operation of coupled reaction in the same reactor to give two useful products over a single catalyst outweighs the cost required for additional units [12, 13]. Therefore, coupling of DHEB to styrene with hydrogenation of nitrobenzene to aniline appears to be an interesting synergetic pair as shown in the scheme. The innovative aspect of the catalytic system discussed here is the utilization of in situ produced hydrogen as a second reagent, allowing for the integrated catalytic transformation of nitrobenzene into aniline without using an external $H_2$ supply. Thus, it helps suppression of the most common side reactions in the primary reaction due to cracking of side chain moiety of ethylbenzene to benzene and ethylene or hydrogenolysis to toluene and methane, coke formation that eliminates the need for periodic regeneration of the dehydrogenation catalysts. Further, aniline produced in the secondary reaction is a valuable chemical commodity for the plastic, rubber processing, herbicide, dye and pigment industries [14].

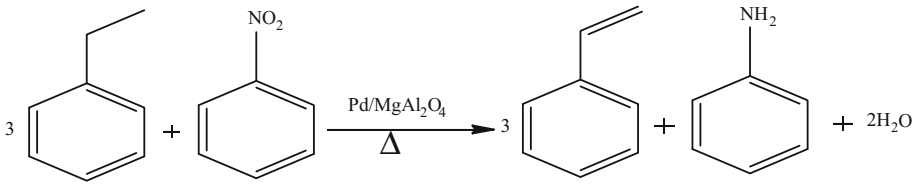


It is a challenging task to develop a sole material to catalyze direct coupling process at higher reaction temperatures, as the catalyst employed for dehydrogenation has to be typically used for hydrogenation reactions as well [15]. Palladium is considered as a primary component in many dehydrogenation catalysts due to its high activity for activating C–H bonds, coupled with an inferior activity for the rupture of C–C bonds, resulting in intrinsically high selectivity toward dehydrogenation. On a Pd surface, only low-coordination number sites (steps, kinks) are able to catalyze the C–C bond breaking, while essentially all Pd sites catalyze the rupture of the C–H bonds. Similarly, Palladium as a primary component is well known for hydrogenation catalyst in many organic transformations. Recently, Guo et al. [16] used palladium catalysts supported on carbon nanotubes, alumina and silica in the hydrogenation of benzaldehyde as well as dehydrogenation of ethylbenzene in the vapor phase. Another undesired side reactions that compete with dehydrogenation are hydrogenolysis and coke formation. Since both, hydrogenolysis and coke formation, are more sensitive to the support structure than dehydrogenation. But, conventionally used supports for Pd catalysts include alumina [17], silica [18, 19], activated carbon, to a lesser extent zeolite and polymers suffer from the disadvantages such as sintering of metal particles, burial of active phase, faster deactivation and coking. The efficient support significantly improves both activity and selectivity of the reaction as observed in coupling of cyclohexanol dehydrogenation with nitrobenzene hydrogenation [20]. Interestingly, some spinel-type mixed metal oxides ($AB_2O_4$) were observed to be interesting materials in hydrogenation and dehydrogenation reactions because of their properties like high thermal and chemical stability and high mechanical resistance. Kustrowski et a1. [21] studied the non-oxidative and oxidative DHEB over Mg–Fe–Cr ternary spinel systems. Similarly, Ji et a1. [22] also investigated Fe-doped $MgAl_2O_4$ spinel catalysts in the O-DHEB reaction. Thus, Magnesium aluminate spinels with neutral as well as basic sites appear to be an efficient catalyst support for palladium active phase for ethylbenzene dehydrogenation, reducing undesired cracking and hydrogenolysis products [23]. Moreover, Magnesium aluminate spinels have a tendency to prevent sintering of precious metals due to their strong metal–support interaction and also provide resistance to coking by reaction media owing to their spinel structure [24].

Hence, a catalytic system based on palladium supported on magnesium aluminate spinel oxide was systematically investigated for its feasibility in the coupling reaction of ethylbenzene with nitrobenzene in a fixed-bed reactor. However, to the best of our knowledge, the performance of supported Pd catalysts for the dehydrogenation of ethylbenzene has not been reported. Here, we are demonstrating the performance of dehydrogenation/hydrogenation activity of $Pd/MgAl_2O_4$ catalysts aiming at higher yield of styrene shifting thermodynamic equilibrium by removing the in situ produced hydrogen for hydrogenation of nitrobenzene. This results in the formation of another useful secondary product (aniline) simultaneously. This avoids additional cost of hydrogen purchasing, transportation and storage for secondary reaction.

## Experimental

### Catalyst preparation

Magnesium aluminate spinel ($MgAl_2O_4$) was prepared by the co-precipitation method [24]. Stoichiometric quantities of Mg $(NO_3)_2{\cdot}6H_2O$ and Al $(NO_3)_3{\cdot}9H_2O$ were dissolved in distilled water and the precipitation of hydroxide was carried out at a controlled pH 9 using 1 M $NH_4OH$ solution at room temperature with vigorous stirring. The precipitate was washed several times with distilled water to remove the excess of nitrate ions. It was dried in an air oven at 373 K for 12 h and then calcined at 1073 K for 8 h to give a spinel phase of $MgAl_2O_4$.

A series of palladium catalysts with varying Pd loadings ranging from 0.25 to 4.0 wt% on this support was prepared by wet impregnation method using an acidified solution of $PdCl_2$ (Aldrich). The samples were dried at 383 K in an air oven for 24 h and finally calcined at 773 K for 5 h in air.

### X-ray diffraction studies

The X-ray diffraction (XRD) patterns were recorded on a Rigaku multiflex diffractometer using Ni filtered CuKα ($\lambda = 0.15406$ nm) radiation of wavelength 1.5418 Å at $2\Theta = 2^{o}$–$80^{o}$ with a scanning rate of $20^{o}$ $min^{-1}$ in a voltage of 40 kV and a current of 100 mA.

### BET surface area

The specific surface areas of the support and catalyst samples were estimated using $N_2$ adsorption–desorption isotherm at 77 K by the multipoint BET (Brunauer–Emmett–Teller) method on an Autosorb-1 instrument (Quantachrome USA). The powder of catalytic samples was first out-gassed at 473 K to ensure a clean surface prior to construction of isotherm. A cross-sectional area (0.164 $nm^2$) of $N_2$ molecule was assumed in the calculation of specific surface areas by BET method.

### Temperature-programmed reduction (TPR)

Temperature-programmed reduction (TPR) experiments were carried out on an Auto Chem 2910 (Micromeritics, USA) instrument. In a typical experiment, Ca. 100 mg of calcined catalyst samples was taken in a *U* shaped quartz sample tube. Prior to TPR studies, the catalyst was pretreated with an inert gas (He, 50 mL/min) at 473 K. After pretreatment, the sample was cooled to ambient temperature and the carrier gas containing of 5 % $H_2$–Ar (50 mL/min) was allowed to pass over the sample while heating from ambient to 873 K at the rate of 10 K/min.

### CO chemisorption

CO chemisorption measurements were also carried out on an Auto Chem 2910 (Micromeritics, USA) instrument. Prior to adsorption measurements, Ca. 100 mg of the sample was reduced in a flow of hydrogen (50 mL/min) at 673 K for 2 h and flushed out subsequently in a pure helium gas flow for an hour at 673 K and cooled to ambient temperature under the same gas flow. CO uptake was determined by injecting pulses of 9.96 % CO balanced helium from a calibrated on-line sampling valve into the helium stream passing over the reduced samples at 673 K.

### X-ray photoelectron spectroscopy (XPS)

The XPS of catalysts was measured on a Kratos-Axis 165, XPS spectrometer with Mg Kα radiation ($h\nu = 1253.6$ eV) at 75 W. The Pd 3d, Mg 2p, and Al 2p core-level spectra were recorded, and the corresponding binding energies were referenced with C 1 s line at 284.6 eV [accuracy within (0.2 eV)]. The background pressure during the data acquisition was kept below $10^{-10}$ bar.

### Transmission electron microscopy (TEM)

Transmission electron microscope (TEM) images of the catalysts were obtained using a Tecnai-12, FEI, The Netherlands at an accelerating voltage of 120 kV. The specimens were prepared by dispersing the samples in methanol using an ultrasonic bath and evaporating a drop of resultant suspension onto the carbon-coated copper grid.

### Temperature-programmed desorption (TPD)

Temperature-programmed desorption of $CO_2$ studies was also conducted on Auto Chem 2910 (Micromeritics, USA) instrument. In a typical experiment for TPD studies, ca. 100 mg of oven-dried sample (dried at 383 K for overnight) was taken in a *U* shaped quartz sample tube. Prior to TPD studies, the catalyst sample was pretreated at 473 K for 30 min by passing pure helium (99.999 %, 50 mL/min). After reduction, the sample was saturated with $CO_2$ in a flow of 10 % $CO_2$ balance He mixture at 303 K with a flow rate of 75 mL/min and was subsequently flushed at 378 K for 1 h to remove physisorbed $CO_2$. TPD analysis was carried out from ambient temperature to 973 K at a heating rate of 10 K/min. The amount of $CO_2$ desorbed was calculated using GRAMS/32 software.

### Catalytic activity studies

The simple dehydrogenation and direct coupling (mixed hydrogenation and dehydrogenation) reactions were carried

out over various Pd/$MgAl_2O_4$ in the range of temperature 673–823 K in a fixed-bed micro-reactor made of quartz (6 mm i.d. and 200 mm long). Ca. 0.5 g of catalyst, diluted with equal amount of quartz grains, was positioned between two layers of quartz wool at the center of reactor. The upper portion of the reactor was filled with quartz grains which served as a pre-heater and mixer for the reactants. A type-K thermocouple enclosed in a quartz thermowell of 3-mm outer diameter was positioned inside the catalyst bed for accurate measurement of the catalyst temperature. Prior to the activity test, the catalyst was reduced in $H_2$ (30 mL/min) at 673 K for 3 h and then passivated under $N_2$ flow (30 mL/min) at 673 K for 0.5 h. After bringing the reactor to required temperature in $N_2$ flow, a mixture of ethylbenzene (EB) and/or nitrobenzene(NB) in the molar ratio of 3:1 at a feed rate of 4.28 mmol $h^{-1}$ was fed into the reactor through a microprocessor-controlled metering pump (Braun, Germany) at atmospheric pressure. The liquid products such as benzene, toluene, styrene, aniline (AN), ethylbenzene and nitrobenzene were collected for every 1 h from ice cold trap and analyzed using an off-line flame ionization detection (FID) gas chromatography (Chemito GC-8510) with a SE-30 (30 m length and 0.53 mm i.d) packed column using Iolar $N_2$ as a carrier gas [25]. The components of liquid products were confirmed by a GC–MS (QP 5050A, Shimadzu Instruments, Japan). Calibration curves of each analyte were constructed using relative response factor against concentration of analyte from gas chromatography signals of prepared mixtures of known composition and used for estimating the percentage of each analyte in the liquid products. In this analysis, tetralin was used as an internal standard substance [26]. A typical calibration plot for determining the percentage of ethylbenzene composition in the mixture of products is shown in Fig. 1. The GC analyzed data were further processed to calculate the conversion and selectivity as mol% using the following Eqs. (1) to (4). Carbon balances of these investigations amounted to ≥95 %.

$$EB_{conv} = [(EB_{fed} - EB_{recovered})/EB_{fed}] \times 100 \quad (1)$$

$$\text{Selectivity of product}_i = [\text{product}_i/(EB_{fed} - EB_{recovered})] \times 100$$
$$\text{where product}_i = \text{styrene, benzene or toluene} \quad (2)$$

$$NB_{conv} = [(NB_{fed} - NB_{recovered})/NB_{fed}] \times 100 \quad (3)$$

$$\text{Selectivity of AN} = [AN/(NB_{fed} - NB_{recovered})] \times 100 \quad (4)$$

## Results and discussion

### XRD studies and BET surface area

The X-ray diffraction patterns of pure $MgAl_2O_4$ and various Pd/$MgAl_2O_4$ catalysts are shown in Fig. 2. All the samples show more intense reflections at $2\theta = 31.2°$, 36.4°, 44.8°, 49.1°, 55.6°, 59.3°, 65.2°, 74.1° and 77.3° (corresponding to $d = 2.86142$, 2.4409, 2.02239, 1.86053, 1.65238, 1.5572, and 1.23456 Å) due to crystallographic peaks of the $MgAl_2O_4$ spinel support (JCPDS-21-1152). The XRD patterns suggest that there are no detectable diffraction peaks representing crystalline PdO in the samples with Pd loading less than 3 wt%. This clearly indicates that palladium oxide species are present in a highly dispersed amorphous state at lower Pd loadings. At lower Pd contents (below 3 wt%), the palladium species are finely dispersed on the $MgAl_2O_4$ spinel. At higher Pd loadings (>3 wt% of Pd), the XRD reflections due to PdO phase are noticed at $2\theta = 33.9°$. The intensities of these reflections are found to increase with the increase of Pd loading, which clearly suggests the crystallinity of PdO at or above 3 wt% loading.

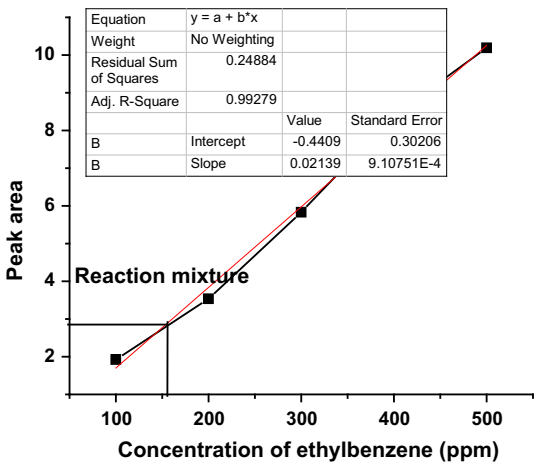


**Fig. 1** Internal standard calibration curve of ethylbenzene

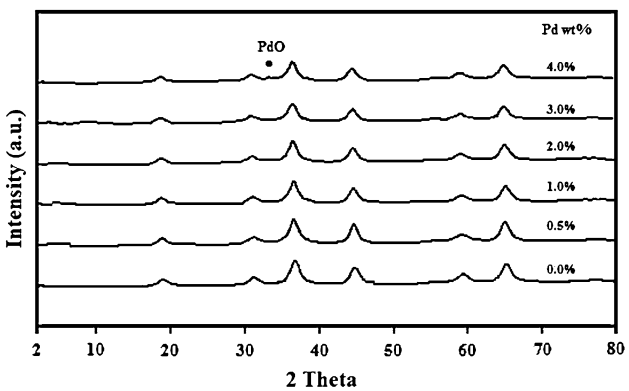


**Fig. 2** Powder X-ray diffraction (XRD) patterns of various PdO/$MgAl_2O_4$ catalysts

The specific surface areas determined by nitrogen physisorption of pure $MgAl_2O_4$ and various $Pd/MgAl_2O_4$ catalysts are presented in Table 1. The specific surface area of the pure $MgAl_2O_4$ support was found to be 126.9 $m^2g^{-1}$ and it decreases as a function of palladium loading. It might be due to partial blocking of the pores of the support by crystallites of palladium oxide as evidenced by XRD.

## $H_2$-TPR studies

The temperature-programmed reduction profiles of various palladium supported on $MgAl_2O_4$ catalysts are shown in the Fig. 3. The TPR profiles of the samples show a reduction peak at above 574 K. This peak is attributed to the reduction of $Pd^{2+}$ or PdO to metallic state of Pd. This reduction temperature is found to be much higher than that of bulk PdO indicating a strong interaction between PdO and $MgAl_2O_4$, which inhibits the reduction. Francova et al. [27] observed similar nature of high temperature reduction of PdO on Pd/Mg(Al)O catalysts. The maximum reduction temperature ($T_{max}$) of this peak varied in the temperature range (574–672 K) depending upon the loading of palladium in $Pd/MgAl_2O_4$ catalysts. The $T_{max}$ value decreases from 672 to 574 K with increasing the palladium content (0.5–4.0 wt%). This implies that at lower Pd loading, the metal particles are highly dispersed as smaller Pd particles and existence of a strong interaction between the palladium and the support.

## CO chemisorption

The physical properties of catalysts such as dispersion, metal surface area and average particle size obtained from CO chemisorption are given in Table 1. The dispersion of Pd was calculated from CO chemisorption using the following equation assuming the cubic particle with five sides exposed to the gas phase.

**Table 1** BET surface area, CO chemisorption and TEM results of various $Pd/MgAl_2O_4$ catalyst

| Pd (wt%) | BET surface area ($m^2/g$) | CO uptake (μmol/g) | Dispersion (%) | Particle size | |
|---|---|---|---|---|---|
| | | | | (nm)[a] | (nm)[b] |
| 0.0 | 126.9 | – | – | – | – |
| 0.5 | 124.4 | 22.4 | 51.2 | 2.2 | 2.0 |
| 1.0 | 120.7 | 27.6 | 30.6 | 4.2 | 4.4 |
| 2.0 | 118.4 | 32.7 | 21.5 | 6.0 | 6.2 |
| 3.0 | 113.8 | 38.5 | 15.5 | 7.6 | 7.9 |
| 4.0 | 108.0 | 45.1 | 13.4 | 8.1 | 8.5 |

[a] Calculated from CO chemisorption method

[b] Calculated from TEM

$$\% \text{ Dispersion} = (\text{Number of surface palladium atoms} \times 100) / \text{Total number of Palladium atoms}$$

$$\text{Average particle size (nm)} = 6000 / (\text{Pd metal area per gram of Pd} \times \text{Pd density})$$

The palladium metal areas were determined using the equation $S_{CO} = nm^S\ X_m\ ns^{-1}$, where $S_{CO}$ is the total metallic surface area, $nm^S$ is the CO consumption and $X_m$ is chemisorption stoichiometry at monolayer coverage, and $ns^{-1}$ is the number of palladium atoms per unit surface area. The CO uptake values of various $Pd/MgAl_2O_4$ catalysts and the other information such as percentage of dispersion, particle size and metal surface area measured at 673 K are given in Table 1. The results clearly suggest that palladium loading and dispersion follow opposite trend. It was found dispersion decreased from 51.2 to 13.4 % with increase in palladium loading from 0.5 to 4.0 wt%, respectively. The high dispersion of Pd observed at lower Pd content may be due to the strong interaction of Pd precursor with oxygen-containing groups of $MgAl_2O_4$ support. It is likely that the deposition may be more on the external surface of the $MgAl_2O_4$ support as Pd content increases in the catalyst. This will reduce the distance among metallic species, thereby promoting agglomerization and decreasing in dispersion. This is in good agreement with XRD results.

## X-ray photoelectron spectroscopy

The binding energies of electrons determined by XPS provide useful information on the oxidation states of

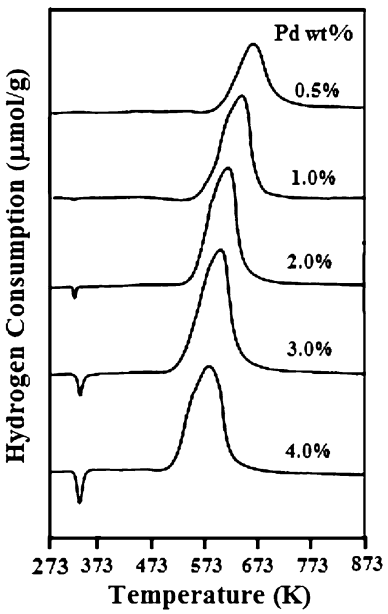


**Fig. 3** Temperature-programmed reduction (TPR) profiles of various $Pd/MgAl_2O_4$ catalysts

different elements. XPS of Pd $3d_{5/2}$ and Pd $3d_{3/2}$ of various calcined Pd/$MgAl_2O_4$ catalysts is shown in Fig. 4, which evaluates the oxidation state and interaction between Pd particle and support. According to the literature, the $Pd^{+2}$ (PdO) $3d_{5/2}$ and $3d_{3/2}$ binding energy values are around ~337.0 and ~342.0 eV, respectively [28]. In the series of catalysts prepared in the present investigation, the doublet peaks of binding energy (BE) for $Pd_{5/2}$ are in the range of 337.4–337.1 and for $Pd_{3/2}$ are 342.8–342.0 eV. These BE values are in good agreement with those reported for PdO in the literature. This implies that $Pd^{2+}O^{2-}$species are much more cationic than the bulk PdO. Usually, this phenomenon can be understood as the strong metal–support interaction (SMSI) effect. Thus, Pd–O bonding does not belong to Pd–O–Pd, but rather to Pd–O–support in the interface, which facilitates an easy electron transfer from Pd to support, producing cationic species. Cationic $Pd^{2+}$($Pd^{n+}O$) species could be formed by the SMSI effect. With increase in palladium loading, there is a slight chemical shift in BE of Pd $3d_{5/2}$ and Pd $3d_{3/2}$ values toward lower side. Chemical shift of BE is generally attributed to the local chemical and physical environment differences. The higher chemical shift of BE in smaller particles is attributed to strong interaction between Pd and support. These results clearly show with increase of Pd loading the metal–support interaction decreases and also dispersion decreases. Voogt et al. [29] also suggested that a chemical shift can be induced by changes in the Pd particle size.

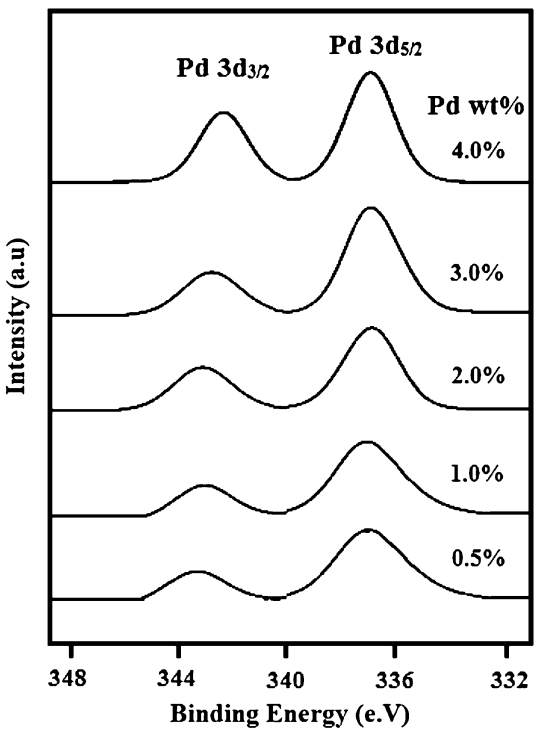


**Fig. 4** Pd 3d XPS spectra of various Pd/$MgAl_2O_4$ Catalysts

From Fig. 4, it is clear that intensities of peak increase with increase of Pd loading, resulting increase in palladium content on the surface of the support. The present XPS results are in well agreement with the dispersion of palladium determined by CO chemisorption and TPR methods.

## Transmission electron microscopy (TEM)

The transmission electron microscopy shown in Fig. 5 allows to visualize the palladium distribution on $MgAl_2O_4$. The dark dots correspond to the palladium particles with heterogeneous distribution. The metal particle size determined by TEM varies from 2.0 to 8.5 nm (Fig. 5a–c) indicating that metal loading facilitated to increase the particle size slightly. It is assumed that it is a consequence of the easier availability of the metal located on the catalyst surface to form clusters. The particle size obtained by chemisorptions measurements which varied from 2.2 to 8.1 nm with increase of palladium loading from 0.5 to 4.0 wt% (Table 1) is comparable with TEM technique which concludes a good agreement between both techniques can be achieved. To study the morphology and size of metal particles distributed over fresh and used catalysts, TEM was performed on 0.5 wt%Pd/$MgAl_2O_4$ catalysts (Fig. 5a–d). The metal size of Pd particles in the fresh catalyst is 2.0 nm while 2.9 nm in used catalyst. The metal particle size of used catalyst has not much significantly changed during course of reaction. Apparently, the coupling reaction (in situ removal of hydrogen) would effectively inhibit the formation of coke by hydrogenolysis which can result the long life time of catalyst.

## Temperature-programmed desorption of $CO_2$

The basicity measurements of Pd/$MgAl_2O_4$ catalysts were carried out by the temperature-programmed desorption of $CO_2$. The $CO_2$ TPD profiles of pure $MgAl_2O_4$ and various Pd/$MgAl_2O_4$ catalysts are shown in Fig. 6. The $CO_2$ uptakes by various catalysts of different basic strengths are reported in Table 2. The desorbed peak of $CO_2$ was deconvoluted into two temperature regions, i.e., 353–473 K consists of weak basic sites and moderate basic sites in the temperature region of 473–673 K [30]. As can be seen from Fig. 6, the TPD profiles are found to be similar for all the samples. The "weak" basic sites are probably associated with desorption of the molecular $CO_2$, "medium" basic sites are corresponding to the $O^{2-}$ and oxygen species from $M^{2+}$–$O^{2-}$ pairs [23]. In the case of supported palladium catalysts, the total basicity decreases with increase of palladium loading. The decrease in basicity at higher Pd loadings might be due to the formation of palladium crystallites. These results are supported by TPR and XRD studies.

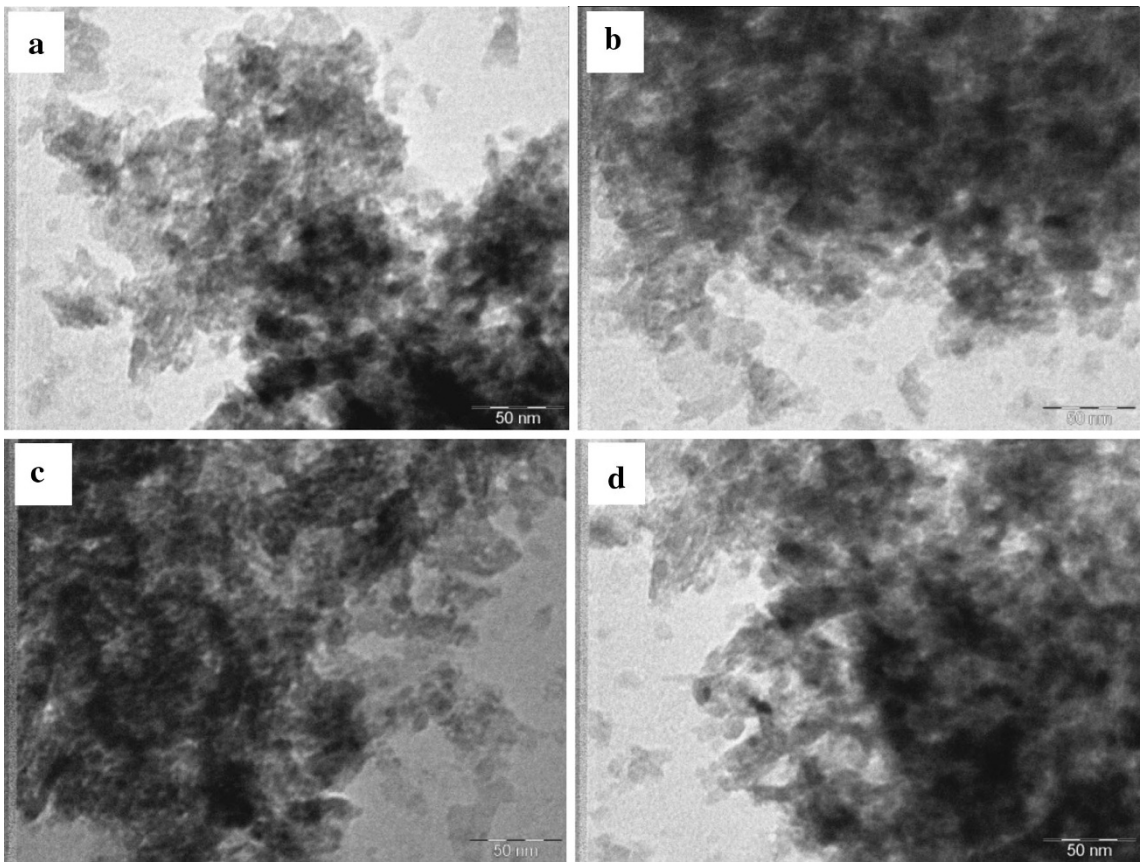


**Fig. 5** Transmission electron microscopy (TEM) images of various $Pd/MgAl_2O_4$ catalyst. **a** 0.5 wt% Pd, **b** 2 wt% Pd, **c** 4 wt% Pd, **d** used 0.5 wt% Pd

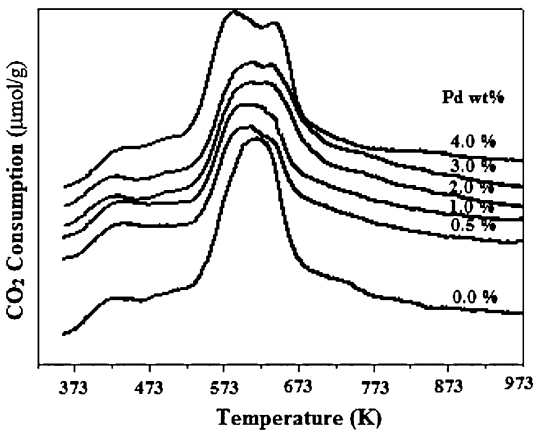


**Fig. 6** Temperature-programmed desorption (TPD) profiles $CO_2$ of various $Pd/MgAl_2O_4$ catalysts

**Table 2** Temperature-programmed desorption results of $CO_2$ of various $Pd/MgAl_2O_4$ catalysts

| Pd loading (%) | $CO_2$ uptake (μmol/g) | | Total $CO_2$ uptake (μmol/g) |
|---|---|---|---|
| | Weak | Medium | |
| 0.0 | 33.2 | 911.3 | 944.5 |
| 0.5 | 51.9 | 945.2 | 997.1 |
| 1.0 | 52.8 | 899.6 | 952.4 |
| 2.0 | 54.2 | 860.6 | 914.8 |
| 3.0 | 56.8 | 831.2 | 888.0 |
| 4.0 | 58.2 | 768.1 | 826.3 |

*Weak* weak basic sites, *medium* moderate basic sites

## Catalytic activity

### Comparison of activity under oxidative and non-oxidative conditions

Simple ethylbenzene dehydrogenation and coupling of ethylbenzene dehydrogenation with nitrobenzene hydrogenation over $MgAl_2O_4$-supported palladium (0.25–4.0 wt%) catalysts at 823 K under atmospheric pressure were investigated. The activity results are shown in Table 3. Conversion of ethylbenzene and selectivity towards styrene on all the catalysts for coupling reactions were much higher than simple dehydrogenation. It can be attributed to in situ removal of hydrogen for participation in the coupling reaction. Similar behavior in the activity of coupling reaction was reported by Bautista et al. [10]. It is

**Table 3** Simple dehydrogenation of ethylbenzene and coupling of EB dehydrogenation with NB hydrogenation over various Pd/$MgAl_2O_4$ catalysts at 823 K

| Without nitrobenzene | | | | | With nitrobenzene | | | | | |
|---|---|---|---|---|---|---|---|---|---|---|
| Catalyst | EB Con. | ST Sel. | Benzene | Toluene | EB Con. | ST Sel. | NB Con. | AN Sel. | Benzene | Toluene |
| (wt%) | (%) | (%) | (%) | (%) | (%) | (%) | (%) | (%) | (%) | (%) |
| 0.25 | 20.8 | 78.4 | 14.2 | 7.4 | 38.2 | 96.1 | 36.6 | 100 | 2.7 | 1.2 |
| 0.5 | 22.4 | 74.3 | 17.5 | 8.2 | 51.8 | 91.4 | 47.3 | 100 | 5.9 | 2.7 |
| 1.0 | 21.9 | 76.4 | 15.8 | 7.8 | 40.3 | 95.8 | 38.6 | 100 | 3.0 | 1.2 |
| 2.0 | 19.8 | 82.9 | 11.4 | 5.7 | 35.8 | 97.1 | 34.7 | 100 | 2.0 | 0.9 |
| 3.0 | 15.9 | 89.2 | 7.6 | 3.2 | 21.6 | 97.9 | 21.1 | 100 | 1.5 | 0.6 |
| 4.0 | 12.9 | 90.1 | 6.9 | 3.0 | 15.9 | 98.2 | 15.6 | 100 | 1.3 | 0.5 |

clear from Table 3 that conversion of ethylbenzene (22.4 %) and selectivity of styrene (74.3 %) in dehydrogenation of ethylbenzene are found to be lower in the absence of NB than its presence over 0.5 wt% Pd/$MgAl_2O_4$ catalyst. The higher conversion of ethylbenzene (51.8 %) and selectivity of styrene (91.4 %) are observed along with 47.3 % conversion of NB to 100 % aniline selectivity in coupling reaction and this trend follows for all other Pd/$MgAl_2O_4$ catalysts. The composition of reaction mixture (EB:ST:Benzene:Toluene:NB:AN) is found to be 36.1:35.5:2.3:1.1:13.2:11.7 under equilibrium conditions.

## Effecting of Pd loading on $MgAl_2O_4$ in catalytic activity

Table 3 shows the effect of Pd loading on coupling of dehydrogenation of ethylbenzene with hydrogenation of nitrobenzene. As the Pd loading increases from 0.25 to 4.0 wt%, the conversion of ethylbenzene and nitrobenzene first increases and then decreases. It is observed that 0.5 wt% Pd/$MgAl_2O_4$ shows an optimum loading for higher conversion of ethylbenzene and it is dropped from 51.8 to 15.9 % and similarly nitrobenzene conversion dropped from 47.3 to 15.6 % with further increase in the palladium loading from 0.5 to 4.0 wt%. Thus, conversions of ethylbenzene decreased progressively with increase in palladium loadings beyond 0.5 wt% are due to low dispersion of Pd and higher particle size, which is clearly observed from the CO chemisorption analysis (Table 1).

## Effect of temperature

Figure 7 shows the catalytic activity of the Pd/$MgAl_2O_4$ catalysts for simple ethylbenzene dehydrogenation and the direct coupling reaction of ethylbenzene dehydrogenation and nitrobenzene hydrogenation in the temperature range of 673–823 K. The increase in the conversion of ethylbenzene from 2.6 to 22.4 % and from 8.2 to 51.8 % takes

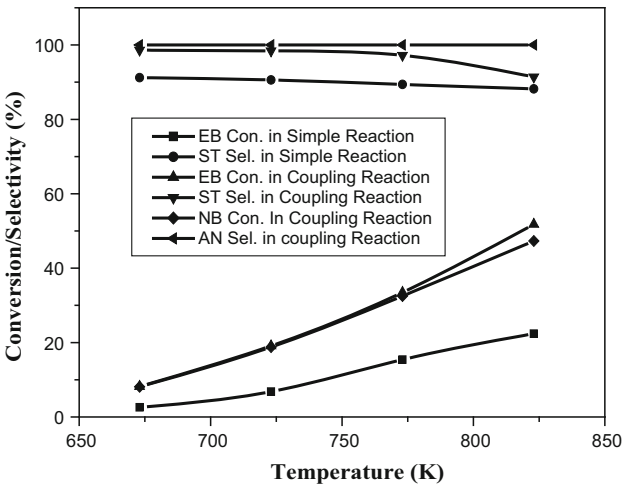


**Fig. 7** Effect of temperature in simple EB dehydrogenation and coupling of EB dehydrogenation with NB hydrogenation over 0.5 wt% Pd/$MgAl_2O_4$ catalyst under equilibrium conditions. Reaction conditions: Weight of the catalyst = 500 mg; molar ratio [EB]/[NB] = 3; flow rate of feed: 4.28 m mol/h

place with the increase in temperature from 673 to 823 K in simple and coupling reactions, respectively. The similar trend is reflected in the conversion of nitrobenzene which is increased from 8.1 to 47.3 % with the production of more in situ hydrogen. The increase in the conversion of ethylbenzene with rise in temperature can be attributed to shift in the equilibrium to the right favoring the forward reaction. The selectivity of styrene decreases with increase in temperature due to formation of higher amount of cracking and hydrogenolysis products such as benzene and toluene. It is interesting to observe that the selectivity of aniline maintained maximum at all the reaction temperatures.

## Effect of time on stream (TOS)

Figure 8 shows the change in the conversion of ethylbenzene/nitrobenzene and selectivity of styrene/aniline with

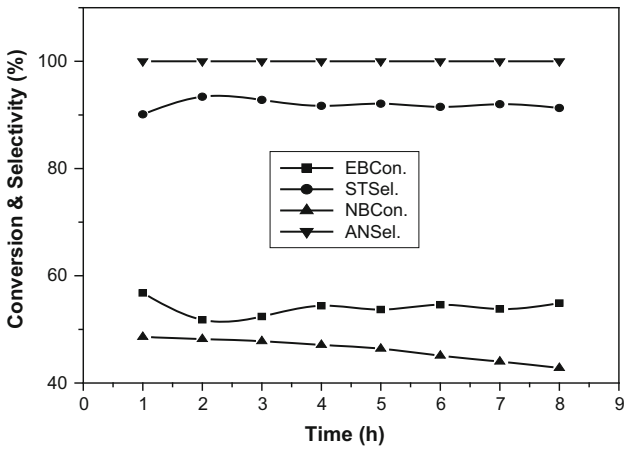


**Fig. 8** Effect of time on stream in the coupling reaction of ethylbenzene with nitrobenzene at 823 K over 0.5 wt% $Pd/MgAl_2O_4$ catalyst. Reaction conditions: Weight of the catalyst = 500 mg; molar ratio [EB]/[NB] = 3; flow rate of feed 4.28 m mol/h

time on stream over a 0.5 wt% $Pd/MgAl_2O_4$ catalyst at 823 K. During the reaction process, the styrene (ST) selectivity kept a very high value (>90 %), however, the initial EB conversion reflected very high (56.8 %) and reached to equilibrium conversion of 51.8 % after 2 h time on stream. It is observed that there is a slow decline in the conversion of nitrobenzene whereas selectivity of aniline is found to be maximum with TOS.

## Conclusion

It was found that the equilibrium conversion could be greatly enhanced by the reaction coupling. When DHEB was coupled with nitrobenzene hydrogenation, the ethylbenzene conversion can reach 51.8 % at 823 K, compared with the conversion of 22.4 % at the same temperature for the simple ethylbenzene dehydrogenation. The effect of dispersion and particle size of palladium of $Pd/MgAl_2O_4$ spinel catalysts is significant in the coupling reaction. It is observed that 0.5 wt% Pd on $MgAl_2O_4$ has exhibited maximum catalytic activity. The reason for the higher activity is attributed to the higher dispersion and lower particle size of Pd as observed from CO chemisorptions, TEM and TPR studies. Thus, $MgAl_2O_4$-supported palladium catalyst is found to be a potential candidate in the coupling reaction for production of styrene from ethylbenzene and aniline from nitrobenzene in a single reactor. The primary experiments on series of catalysts proved that the reaction coupling was an effective measure to improve the ethylbenzene dehydrogenation, although much more work is still necessary to develop proper catalysts for the coupling reactions.

**Acknowledgments** The authors thank Director, IICT, Hyderabad, for her encouragement. One of the authors (YDHK) thanks University Grants Commission (UGC), New Delhi, India for the award of research fellowship (Grant number 20-6/2008 (II), EU-IV).



## References

1. Brydson JA (1999) Plastics materials, 7th edn. Butterworth-Heinemann, Oxford
2. Lee H (1973) Iron oxide catalysts for dehydrogenation of ethylbenzene in the presence of steam. Catal Rev 8:285–305
3. Tiscareno-Lechuga F, Hill CG Jr, Anderson MA (1993) Experimental studies of the non-oxidative dehydrogenation of ethylbenzene using a membrane reactor. Appl Catal A Gen 96:33–51
4. Abashar MEE (2004) Coupling of ethylbenzene dehydrogenation and benzene hydrogenation reactions in fixed bed catalytic reactors. Chem Eng Proc 43:1195–1202
5. Abdalla BK, Elnashaie SSEH (1993) A membrane reactor for the production of styrene from ethylbenzene. J Membr Sci 85:229–239
6. Zhao TJ, Sun WZ, Gu XY, Ronning M, Chen D, Dai YC, Yuan WK, Holmen A (2007) Rational design of the carbon nanofiber catalysts for oxidative dehydrogenation of ethylbenzene. Appl Catal A Gen 323:135–146
7. Gaspar JN, Vadekar M, Pasternak IS, Cohen AD (1975) $SO_2$ promoted oxidative dehydrogenation of ethylbenzene. Can J Chem Eng 53:74–78
8. Burri DR, Choi KM, Han DS, Sujandi, Jiang N, Burri A, Park SE (2008) Oxidative dehydrogenation of ethyl benzene to styrene with $CO_2$ over $SnO_2$–$ZrO_2$ mixed oxide nanocomposite catalysts. Catal Today 131:173–178
9. Towler G, Lynn S (1994) Novel applications of reaction: use of carbon dioxide to shift the equilibrium of dehydrogenation reactions. Chem Eng Sci 49:2585–2591
10. Bautista FM, Campelo JM, Garcia A, Luna D, Marinas JM, Quiros RA, Romero AA (1999) Gas-phase oxydehydrogenation of ethylbenzene with nitrobenzene by hydrogen transfer catalyzed reaction to produce styrene and aniline. Catal Lett 60:229–235
11. Sun A, Qin Z, Wang J (2002) Reaction coupling of ethylbenzene dehydrogenation with nitrobenzene hydrogenation. Catal Lett 79:33–37
12. Abo-Ghander NS, Grace JR, Elnashaie SSEH, Lim CJ (2008) Modeling of a novel membrane reactor to Integrate dehydrogenation of ethylbenzene to styrene with hydrogenation of nitrobenzene to aniline. Chem Eng Sci 63:1817–1826
13. Qin Z, Liu J, Sun A, Wang J (2003) Reaction coupling in the new processes for producing styrene from ethylbenzene. Ind Eng Chem Res 42:1329–1333
14. Chenier PJ (2002) Survey of industrial chemistry, 3rd edn. Kluwer Academic/Plenum, New York
15. Bartholomew CH, Farrato RJ (2006) Fundamentals of industrial catalytic process, 2 edn. Wiley, New York
16. Guo XF, Jang DY, Jang HG, Kim GJ (2012) Hydrogenation and dehydrogenation reactions catalyzed by CNTs supported palladium catalysts. Catal Today 186:109–114
17. Skotak M, Lomot D, Karpinski Z (2002) Catalytic conversion of $C_6$-alkanes over $Pd/Al_2O_3$ catalysts the effect of support acidity. Appl Catal A Gen 229:103–115

18. Yuranov I, Moeckli P, Suvorona E, Buffat P, Minsker L, Reuken A (2003) Pd/$SiO_2$ catalysts: synthesis of Pd nanoparticles with the controlled size in mesoporous silicas. J Mol Catal A Chem 192:239–251
19. Heidenrich R, Krauter J, Pietsch J, Kohler K (2002) Control of Pd leaching in Heck reactions of bromoarenes catalyzed by Pd supported on activated carbon. J Mol Catal A Chem 182:499–509
20. Pramod CV, Suresh M, Mohan V, Sridevi B, Burri DR, Rama Rao KS (2012) Coupling of cyclohexanol dehydrogenation-nitrobenzene hydrogenation over MgO–$Al_2O_3$ Hydrotalcite supported Cu catalysts: effect of Cu loading. Curr Catal 1:140–148
21. Kustrowski P, Chmielarz L, Rafalska-Lasocha A, Dudek B, Pattek-Janczyk A, Dziembaj R (2006) Catalytic reduction of $N_2O$ by ethylbenzene over novel hydrotalcite-derived Mg–Cr–Fe–O as an alternative route for simultaneous $N_2O$ abatement and styrene production. Catal Commun 7:1047–1052
22. Ji M, Zhang X, Wang J, Park SE (2013) Ethylbenzene with $CO_2$ over Fe doped $MgAl_2O_4$ spinel catalysts: synergy effect between $Fe^{+2}$ and $Fe^{+3}$. J Mol Catal A Chem 371:36–41
23. Batistaa AHM, Ramos FSO, Braga TP, Limab CL, Sousab FF, Barros EBD, Filho JM, Oliveirac AS, Sousac JR, Valentinia A, Oliveiraa AC (2010) Mesoporous $MAl_2O_4$ (M = Cu, Ni, Fe or Mg) spinels: Characterisation and application in the catalytic dehydrogenation of ethylbenzene in the presence of $CO_2$. Appl Catal A Gen 382:148–157
24. Guo J, Lou H, Zhao H, Chai D, Zheng X (2004) Dry reforming of methane over nickel catalysts supported on magnesium aluminate spinels. Appl Catal A Gen 273:75–82
25. Harikrishna Y, Pavankumar V, Chary KVR, Venkat Rao V (2014) Characterization and reactivity of Pd supported on $ZnAl_2O_4$ catalysts for direct coupling of ethylbenzene dehydrogenation with nitrobenzene hydrogenation. Indian J Chem 53A:459–466
26. Sekine Y, Watanabe R, Matsukata M, Kikuchi E (2008) High performance of Fe–K oxide catalysts for dehydrogenation of ethylbenzene to styrene with an aid of ppm-order Pd. Catal Lett 125:215–219
27. Francova D, Tanchoux N, Gerardin C, Trens P, Prinetto F, Ghiotti G, Tichit D, Coq B (2007) Hydrogenation of 2-butyne-1,4-diol on supported Pd catalysts obtained from LDH precursors. Micro Meso Mater 99:118–125
28. Naresh D, Kumar VP, Harisekhar M, Nagaraju N, Putrakumar B, Chary KVR (2014) Characterization and functionalities of Pd/hydrotalcite catalysts. Appl Surf Sci 314:199–207
29. Voogt EH, Mens AJM, Gijzeman OLJ, Geus JW (1996) XPS analysis of palladium oxide layers and particles. Surf Sci 350:21–31
30. Peng SY, Xu ZN, Chen QS, Wang ZQ, Chen Y, Lv DM, Lu G, Guo GC (2014) MgO: an excellent catalyst support for CO oxidative coupling to dimethyl oxalate. Cat Sci Tech 4:1925–1930